Research Article

Ling Tan, Qiandan Fan, Fei Huang, Xin Tian, Wei Wei, Tongxin Bian, Yifan Guo*, Xiaoling Xu, and Zuowan Zhou*

Excited-state geometry relaxation of pyrenemodified cellulose nanocrystals under UV-light excitation for detecting Fe³⁺

https://doi.org/10.1515/ntrev-2022-0141 received April 14, 2022; accepted May 26, 2022

Abstract: Capturing and detecting Fe³⁺ ions in aqueous solution is of great significance in biological systems as well as the water treatment industry. Herein, pyrenemodified cellulose nanocrystal (CNC-1-Pyr) acting as a fluorescent probe was prepared by a one-step esterification reaction, which shows geometry relaxation under UV-light excitation. Experiments and density functional theory-based simulations revealed that the structural geometry relaxation is controlled by the electron excitation and fluorescence emission. The S1 state of CNC-1-Pyr provides a conformation match for coordination with Fe³⁺ under the excitation of UV light, facilitating the detecting and capturing of Fe³⁺ efficiently.

Wei Wei: Key Laboratory of Advanced Technologies of Materials (Ministry of Education), School of Materials Science and Engineering, Southwest Jiaotong University, Chengdu, Sichuan 610031, China; Yibin Institute of Southwest Jiaotong University, Yibin, Sichuan 644000, China

Keywords: pyrene-modified cellulose nanocrystals, UVlight excitation, Fe³⁺ ions

1 Introduction

Iron, as an irreplaceable role, has long been widely distributed in natural environment and organisms [1,2]. It is of importance to achieve highly sensitive and specific detection of Fe³⁺, which is closely associated with some key issues such as product quality and sewage discharge. Various techniques involving voltammetric determination [3], inductively coupled plasma-mass spectrometry [4], atomic absorption spectrometry [5], and chemical probes [6-9] have been employed for detecting Fe³⁺. Among these strategies, the fluorescent probes gain considerable attention because of its advantages in superior selectivity, high sensitivity, and rapid response [10,11]. Once contacting with target ions, the designed probes show phenomena such as isomer tautomerism, electron charge transfer [12], and formation or fracture of dynamic chemical bonds [13], which lead to the change of fluorescence spectrum [14-17]. Therefore, it is available for identifying the target ions, indicating a device-independent method for the qualitative detection of Fe³⁺.

Pyrene and its derivatives have been proved to be superior candidates for designing fluorescent probes [18]. Benefiting from their intrinsic structures of polycyclic aromatic hydrocarbons, these probes have advantages in high quantum yield and long fluorescence lifetime [19-22]. Moreover, the emitted fluorescence locates in the visible bands, facilitating the observation of sensing signals. However, the aromatic structure of pyrene results in poor solubility in aqueous solution. These aggregated pyrene molecules lost the photoluminescence ability, known as the aggregation caused fluorescence quenching [23]. Thus, pyrene and its derivatives are always chemically modified for achieving applications as fluorescent probes. For example, pyrene

License.

^{*} Corresponding author: Yifan Guo, Key Laboratory of Advanced Technologies of Materials (Ministry of Education), School of Materials Science and Engineering, Southwest Jiaotong University, Chengdu, Sichuan 610031, China; Yibin Institute of Southwest Jiaotong University, Yibin, Sichuan 644000, China, e-mail: yfguo@swjtu.edu.cn

^{*} Corresponding author: Zuowan Zhou, Key Laboratory of Advanced Technologies of Materials (Ministry of Education), School of Materials Science and Engineering, Southwest Jiaotong University, Chengdu, Sichuan 610031, China; Yibin Institute of Southwest Jiaotong University, Yibin, Sichuan 644000, China; Institute of Frontier Science and Technology, Southwest Jiaotong University, Chengdu, Sichuan 610031, China, e-mail: zwzhou@swjtu.edu.cn Ling Tan, Qiandan Fan, Fei Huang, Tongxin Bian, Xiaoling Xu: Key Laboratory of Advanced Technologies of Materials (Ministry of Education), School of Materials Science and Engineering, Southwest Jiaotong University, Chengdu, Sichuan 610031, China Xin Tian: College of Materials Science and Engineering, Sichuan University, Chengdu, Sichuan 610065, China

was grafted onto cellulose nanocrystals (CNCs) to achieve sensitive detection for distinguishing Fe³⁺ [24]. Actually, it is a two-stage detection process, including capturing Fe³⁺ and subsequent fluorescence quenching. The latter has been empirically attributed to electron transfer-induced quenching and few discussions talking about the former.

In this study, we synthesized CNC-1-Pyr as a fluorescent probe by one-step esterification. Considering the fact that light-excited molecules always undergo geometry relaxations, we speculated that the excited-state geometry relaxation of CNC-1-Pyr from S0 to S1 state may affect their efficiency in capturing Fe³⁺. A series of experiments and simulations were performed to investigate the geometry relaxation under UV-light excitation, further exploring their influence on capturing and detecting Fe³⁺. We believe that this will bring to light the potential mechanisms responsible for the special complex of excited fluorescent molecules with ions, such as Fe³⁺.

2 Experimental methods

2.1 Materials

CNCs were purchased from Science-K Nanotechnology Co., Ltd. 1-Pyrene carboxylic acid (1-Pyr) was purchased from Macklin (Shanghai, China). *N,N*-Dimethylformamide (DMF) and kinds of metal salts (including LiCl, NaCl, KCl, NiCl₂, NH₄Cl, CoCl₂·6H₂O, BaCl₂, ZnCl₂, FeCl₂·4H₂O, FeCl₃·6H₂O, CuCl₂·2H₂O, MnCl₂·4H₂O, SnCl₂, Mg(NO₃)₂·6H₂O, Pb(NO₃)₂, CaCl₂, AlSO₄·18H₂O, and K₂Cr₂O₇) were supplied by Chengdu Kelong Chemical Reagent Co. (Chengdu, China). *N,N'*-Dicyclohexylcarbodiimide (DCC) and 4-dimethylaminopyridine (DMAP) were provided by Aladdin (Shanghai, China). All the reagents and solvents were of analytical grades and used as received.

2.2 Synthesis of pyrene-modified CNCs

The pyrene-modified CNCs were prepared by a one-step esterification reaction between 1-Pyr and CNCs. Generally, CNCs (1 g) and 1-Pyr (0.09 g) were added into anhydrous DMF (80 mL) with ultrasonication to achieve a homogeneous suspension. Then, 0.53 g of DCC and 1.21 g of DMAP were added to the suspension. It was heated to 155°C and kept for 2h with continuous magnetic stirring. All these processes were performed avoiding light. After the reaction, the suspension was cooled down to room temperature.

The precipitates were separated by vacuum filtration and then washed with DMF and water three times to remove the unreacted 1-Pyr. The obtained products were dispersed into water and dialyzed against water for 1 week. Finally, they were centrifuged concentrated (8,000 rpm, 10 min) followed by freeze-drying to obtain white powder referred to as CNC-1-Pyr.

2.3 Characterizations

The morphologies of raw material CNCs and CNC-1-Pvr were observed by transmission scanning electron microscope (TEM: Thermo scientific, USA), Fourier transform infrared (FT-IR; Bruker, Germany) spectra were collected on a Tensor II, with a spectral resolution of 2 cm⁻¹ in the range of 4,000–400 cm⁻¹. The C element variation during the synthesis process was analyzed by X-ray photoelectron spectroscopy (XPS; Thermo scientific, USA). Raman (RENISHAW; InVia, England) spectra were recorded with a spectral resolution of 2 cm⁻¹. The excitation wavelength used for the test was 532 nm. The crystal structures were studied by X-ray diffraction (XRD; Empyrean, Netherlands) with Cu Kα radiation. The UV-visible absorbance spectra and fluorescence emission spectra were collected from U-3310 (UV-Vis, SHIMADZU, Japan) and F-2700 spectrometers (FLS; Hitachi, Japan), respectively.

2.4 Detection of Fe³⁺ aqueous solution

CNC-1-Pyr solution of 0.5 mL (0.05 mg/mL) was mixed with 0.5 mL Fe³⁺ aqueous solution. The Fe³⁺ aqueous solution was prepared by dissolving a given mass of FeCl₃·6H₂O into deionized water. The concentration of Fe3+ (labeled as $c(Fe^{3+})$) is in the range of 0–90,000 μ mol/L. Fluorescence emission spectra of the mixed solution were characterized to investigate the relationships between fluorescence intensities and c(Fe³⁺). Some other kinds of metal salts including LiCl, NaCl, KCl, NiCl₂, NH₄Cl, CoCl₂·6H₂O, BaCl₂, ZnCl₂, FeCl₂·4H₂O, FeCl₃·6H₂O, CuCl₂·2H₂O, MnCl₂·4H₂O, SnCl₂, Mg(NO₃)₂·6H₂O, Pb(NO₃)₂, CaCl₂, AlSO₄·18H₂O, K₂Cr₂O₇, and their mixture with Fe3+ were subjected to a similar operation, for investigating the specific detection ability of CNC-1-Pyr. The limit of detection (LOD) [12] is calculated based on the three times standard deviation method. The formula for calculating LOD is described in the following equation:

$$LOD = 3\sigma/m, \tag{1}$$

where σ stands for the standard deviation of the fluorescence emission intensity of blank CNC-1-Pvr and *m* is the slope of the linear fits drawn by the fluorescence intensity (420 nm) as a function of Fe³⁺ concentration.

2.5 Computational details

The molecular models including CNC, 1-Pyr, CNC-1-Pyr, and their complexes were constructed in Gauss View 5.0. Structural optimizations of these models were first performed based on the density functional theory (DFT). The single-point calculations for the optimized models were subsequently implemented to obtain their molecular orbitals and density of states (DOS). Their electron excitation was calculated based on time-dependent-DFT (TD-DFT). All simulations were implemented by Gaussian 16 program [25] using PBE1PBE exchange-correlation functional in conjunction with 6-311g** basis set. The wave functions were handled with Multiwfn 3.8 [26]. Molecular models and orbitals were rendered by Visual Molecular Dynamics software [27].

3 Results and discussion

First, the pyrene-modified CNCs were prepared, taking advantage of the abundant hydroxyl groups in the intrinsic cellulose molecule [28,29]. 1-Pyrene carboxylic acids (1-Pyr) were covalently grafted onto the surface of CNCs by a onestep esterification reaction. The grafting ratio was calculated based on the UV-Vis colorimetric method [30] (details in Supporting Information) to be 3.89 wt% (Figure S1). TEM images show that the surface grafting did not affect the original spindle-shaped morphologies of CNCs (Figure 1a and b). FT-IR spectrum of CNCs, depicted in Figure 1c, displays the typical absorption peaks of natural cellulose [31]. However, a newly emerging peak observed at around 1,670 cm⁻¹ in the CNC-1-Pyr spectrum (Figure 1d), when de-convoluted, shows the presence of C=O stretching vibration from the ester bonds. Raman shift at around 1650 cm⁻¹ (Figure 1e) was also observed in the spectrum of CNC-1-Pyr, which is induced by the conjugated benzene rings in 1-Pvr [32]. Moreover, explicit blue shifts are observed in Figure S2a for the -CH₂- stretching vibration in the modified CNCs with respect to the original one. Moreover, the symmetrical vibration of C-H shifts from 2,851 cm⁻¹ in the original CNCs to 2,854 cm⁻¹ in the modified one, whereas the antisymmetric one shifts from 2,902 to 2923 cm⁻¹. As

the -CH₂- group is adjacent to the formed ester bond, the presence of C=O moiety reinforced the C-H bonds in -CH₂by conjugating the π -electron clouds from pyrene, as illustrated in Figure S2b.

XPS characterization provides additional evidence for the esterification. Compared with the raw material CNCs, emerging of a new peak located at a binding energy of 289.21 eV in CNC-1-Pyr was attributed to the C=O bond in the ester group (Figure 1f and g). The C-C/C-H area ratio of de-convoluted peaks increased from 14 to 39% after the grafting also proves the esterification grafting of 1-Pvr onto CNCs.

The crystal structure of raw material CNCs and fluorescent probe CNC-1-Pyr was characterized by XRD, as shown in Figure 1h. Pyrene-modified CNCs present a similar diffraction pattern to CNCs. The peaks located at $2\theta = 15.2^{\circ}$, 17° , 22.5° , and 34.5° correspond to the crystal planes (110), (110), (200), and (004), respectively [33]. Similar to the CNCs, the chemically modified product CNC-1-Pyr exhibits a typical natural cellulose I crystal form. The above results indicate that grafting has little influence on the complete crystal structure of CNCs.

The optical absorption and photoluminescence of pyrene-modified CNCs were then evaluated. Figure 2a and f presents the digital photos of CNCs, 1-Pyr, and CNC-1-Pyr when exposed either to natural or UV light. Their UV-vis and fluorescence emission spectra are presented in Figure 2g and h, respectively. Due to the presence of abundant hydrophilic hydroxyls and ether bonds, CNCs can be easily dispersed in aqueous medium. The transparent solution of CNCs displays hardly any excitation or fluorescence emission peak in the tested wavelength range (Figure 2g₁ and h₁). As for 1-Pyr, the three major adsorption peaks located at about 240.0, 275.5, and 341.5 nm (Figure 2g₂) were attributed to the electronic transition around the Fermi level, as depicted by the simulation results (Figure S3). The subsequent de-excitation resulted in fluorescence emission, as detected in Figure 2h₂. However, the low solubility of 1-Pyr results in the formation of aggregates in the aqueous solution, consequently, leading to inhomogeneous fluorescent solution (Figure 2c and d). The shoulder peaks observed in UV-vis spectra may also originate from the presence of these aggregates. After grafting, the pyrene-modified CNCs still hold an excellent dispersion ability in the aqueous medium. The slightly blue shift of the electronic excitation peaks (Figure 2g₃) occurred due to the enlarged gap (Figure S4) between the highest occupied molecular orbital and the lowest unoccupied molecular orbital. Bright and homogeneous blue fluorescence was observed from the CNC-1-Pyr solution, as displayed in Figure 2f. Furthermore, the fluorescence

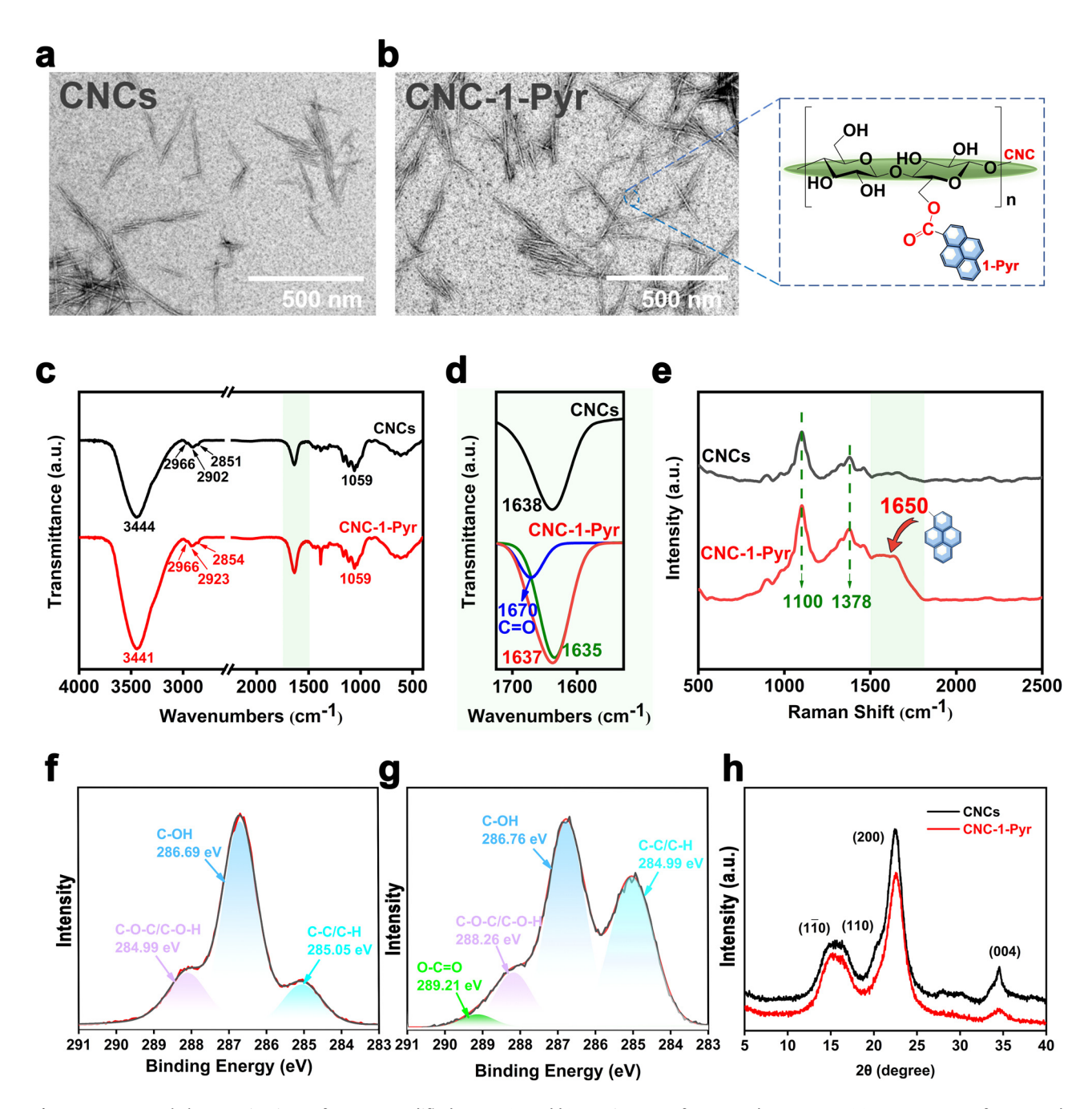


Figure 1: Structural characterizations of pyrene-modified CNCs: (a and b) TEM images of CNCs and CNC-1-Pyr, (c) FT-IR spectra of CNCs and CNC-1-Pyr, (d) enlarged absorption peaks in a range of 1,530–1,730 cm⁻¹ as marked in (c), (e) Raman spectra of CNCs and CNC-1-Pyr (f and g) high-resolution XPS of C 1s in (f) CNCs, (g) CNC-1-Pyr, and (h) XRD of CNCs and CNC-1-Pyr.

emission spectra shown in Figure $2h_3$ exhibit characteristic bands located at 387.4, 406.8, and 433.4 nm, which attributed to the fluorescent molecule 1-pyr. This is consistent with the above structural characterization results, and the esterification reaction was successfully carried out.

DFT-based simulations were performed to investigate the photoluminescence and quenching behavior of the interaction between CNC-1-Pyr and Fe^{3+} . First, the molecular

structures of CNC-1-Pyr in the ground state (S0 state) and the first excited state (S1 state) are presented in Figure 2i. The cellulose molecule chains shown here are rendered using "glass bubble" models. One can notice that there is a conspicuous geometry relaxation during UV-light excitation and fluorescence emission, which is dominated by the rotation of the ester bonds. It is well known that the rotation of C–C and C–O bonds in an ester bond is generally permissible.

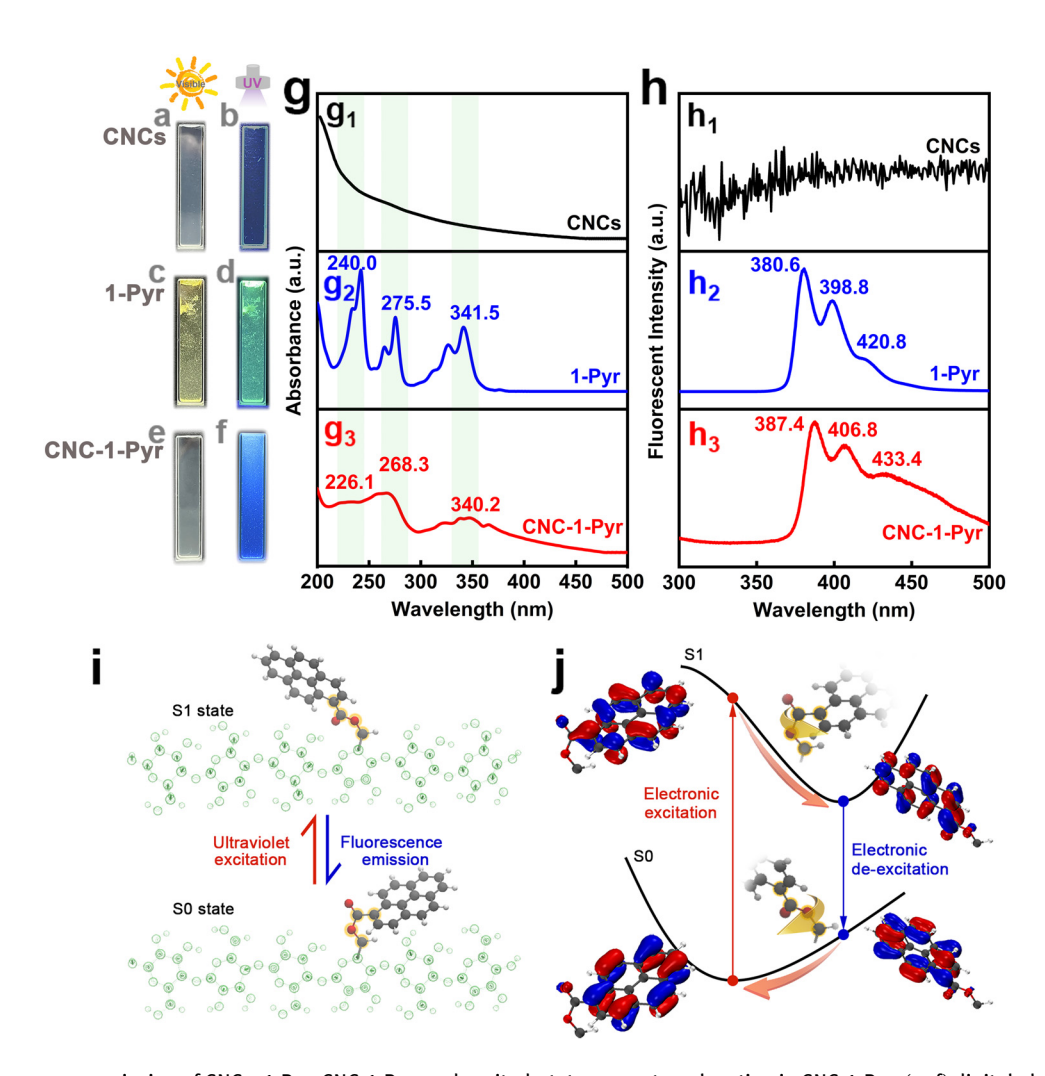


Figure 2: Fluorescence emission of CNCs, 1-Pyr, CNC-1-Pyr, and excited-state geometry relaxation in CNC-1-Pyr: (a-f) digital photos of (a and b) CNCs, (c and d) 1-Pyr, and (e and f) CNC-1-Pyr under (a, c, and e) natural light or (b, d, and f) UV light. (g) UV-vis spectra and (h) fluorescence emission spectra of $(g_1$ and $h_1)$ CNCs, $(g_2$ and $h_2)$ 1-Pyr, and $(g_3$ and $h_3)$ CNC-1-Pyr. (i) Stable conformation of CNC-1-Pyr in S0 and S1 state. (j) Transformation of electronic and molecular structures along S0/S1 potential energy surface during excitation, and de-excitation.

However, distinct steric hindrance may exist during the rotation process due to the existence of the large pyrene groups. Our simulation results calculated based on TD-DFT demonstrate that the rotation of ester bonds in CNC-1-Pyr is allowed thermodynamically. The rotation of dihedral angle reaches up to –174° when excited from S0 to S1 state. Furthermore, molecular orbitals around the Fermi level are presented in Figure 2j to illustrate the structural relaxation process. A local excitation dominated by $\pi\to\pi^\star$ transition is recognized during the UV-induced electronic excitation. The excited electron clouds diffuse around the ester bond, resulting in the geometry relaxation along with the S1 potential energy surface. The ester bond consequently rotates to achieve a low-energy conformation, driving the swing of the pyrene segment. A similar phenomenon

occurs during the electronic de-excitation throughout the fluorescence emission process.

It is wondered whether metal ions can affect the fluorescence property of CNC-1-Pyr. So various kinds of metal ions including Li⁺, Na⁺, K⁺, Ni⁺, NH₄⁺, Co²⁺, Ba²⁺, Zn²⁺, Fe²⁺, Fe³⁺, Cu²⁺, Mn²⁺, Sn²⁺, Mg²⁺, Pb²⁺, Ca²⁺, Al³⁺, and Cr⁶⁺ were introduced into the CNC-1-Pyr solution, as presented in Figure S5 and Figure 3a. Except for Fe³⁺, these metal ions almost exhibit no influence on the fluorescence emission spectrum of CNC-1-Pyr. That is to say, Fe³⁺ seems to be the unique and excellent fluorescent quencher for CNC-1-Pyr. Besides, the quenching effect of Fe³⁺ shows good resistance to the interference of other metal ions mentioned above, as shown in Figure S5 (*e.g.*, "Li⁺⁺ Fe³⁺," "Na⁺⁺ Fe³⁺", *etc.*).

The CNC-1-Pyr solution displays a broad linear response range from 1 to 1,000 μ mol/L (Figure 4b) for quantitative detection of Fe³⁺. The linear regression equation is fitting to be $I_0/I=0.0048\,\mathrm{C}+1.0525$ (R=0.9964). Thus, the quenching constant K_{SV} is calculated to be 4,800 mol/L and the combination ratio of CNC-1-Pyr and Fe³⁺ is about 1:1. In addition, the LOD is as low as 0.3374 μ mol/L with a signal-to-noise ratio of 3. As compared to recently reported fluorescent probes or chemical sensors (Table S1), CNC-1-Pyr possesses a large detection range and relatively high detection sensitivity, indicating its application potential for specific detection Fe³⁺ in the aqueous solution.

To reveal the mechanism of specific quenching, the conformation of the optimized Fe^{3+} @CNC-1-Pyr complex is exhibited in Figure 3b. The Fe^{3+} is found to be triangularly anchored by the synergistic effect of the carbonyl group in the ester bond and the hydroxyl groups in the cellulose molecule. According to the DOS of free Fe^{3+} and Fe^{3+} @CNC-1-Pyr complex shown in Figure 3c, the halffull 3d orbit in Fe^{3+} captures an additional electron from

the adjacent O atoms, as marked by the arrow, which indicates the formation of the coordination complex between CNC-1-Pyr and Fe^{3+} . Therefore, the mechanism of identifying Fe^{3+} ions can be reasonably explained by the electron transfer process occurring between the excited pyrene groups and Fe^{3+} ions [6,7,34–36]. In addition, the higher the Fe^{3+} ion concentration, the greater the redox reaction between the two, and the fluorescence intensity quenching clearer consequently.

Further experiments demonstrate that there are two possible routes for the complexing of Fe³⁺ and CNC-1-Pyr, as shown in Figure 5. The first case, if CNC-1-Pyr is primarily excited into the S1 state by UV irradiation, and there has an immediate fluorescence quench of the mix solution (Fe³⁺ and CNC-1-Pyr), followed by quick precipitation of CNC-1-Pyr in the next 10 min (Figure 5b1 and 4). The red arrows in Figure 5b point out the complex precipitation. On the other hand, almost no changes can be observed after adding Fe³⁺ without UV irradiation (natural light), as shown in Figure 5b5 and 8. Note that the

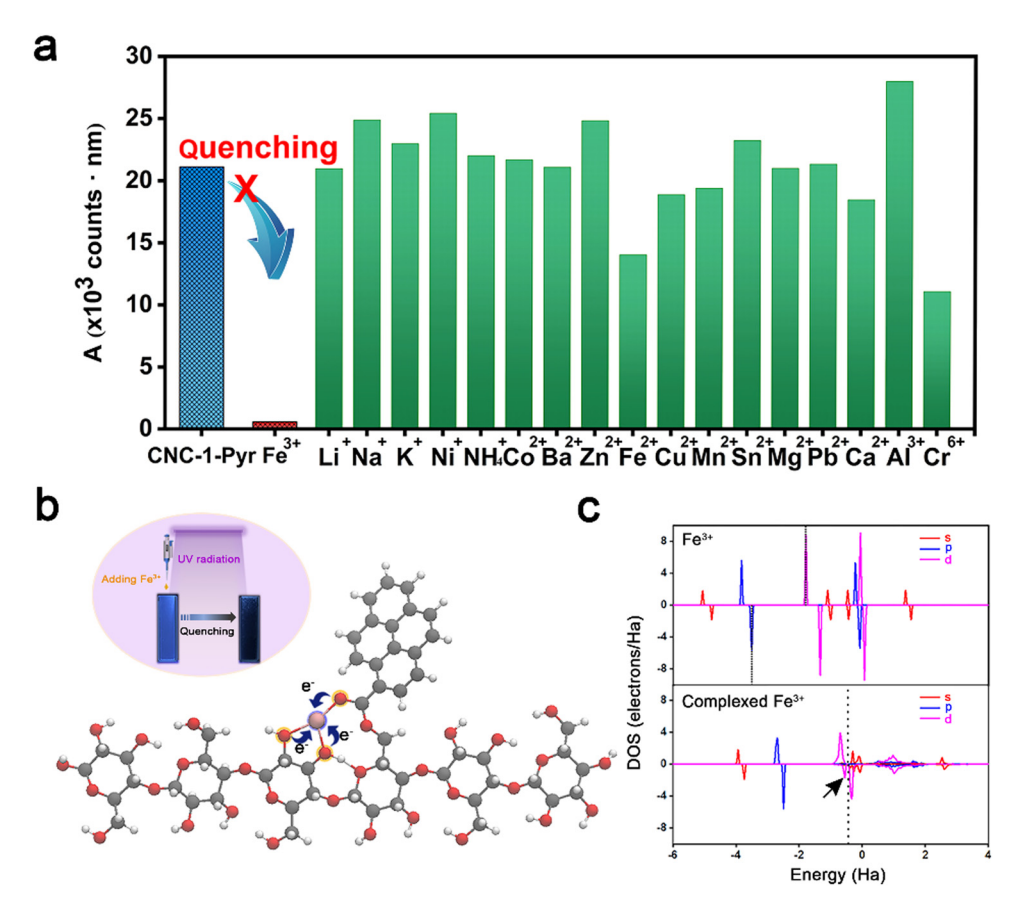


Figure 3: Fluorescence quenching of CNC-1-Pyr for specific detection of Fe³⁺: (a) integral area of emission peaks calculated from the fluorescence emission spectra, (b) stable conformation of CNC-1-Pyr after complexing with Fe³⁺. The inset is the digital photos of the CNC-1-Pyr solution before and after fluorescence quenching. (c) DOS of free Fe³⁺ and Fe³⁺ @CNC-1-Pyr complex. The dotted lines refer to the Fermi levels. The arrow points out the captured electron from adjacent O atoms.

2532 — Ling Tan et al. DE GRUYTER

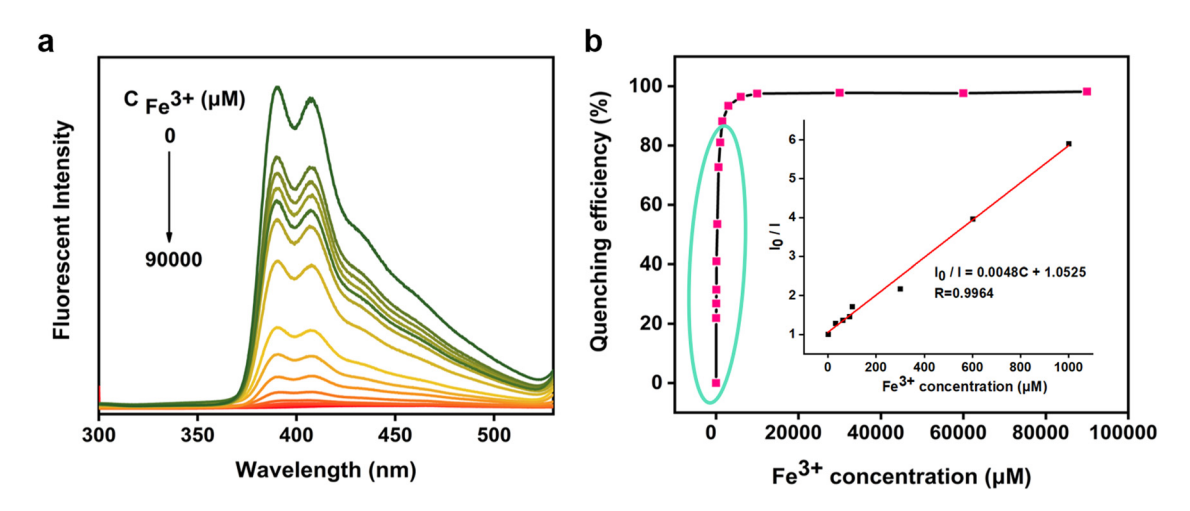


Figure 4: Linear range and the LOD of CNC-1-Pyr solution for quantitative detection of Fe³⁺: (a) fluorescence emission spectra of CNC-1-Pyr solution mixing with Fe³⁺ solution and (b) calculated quenching efficiency of CNC-1-Pyr solution, the inset is Stern-Volmer plot of the quenching behavior.

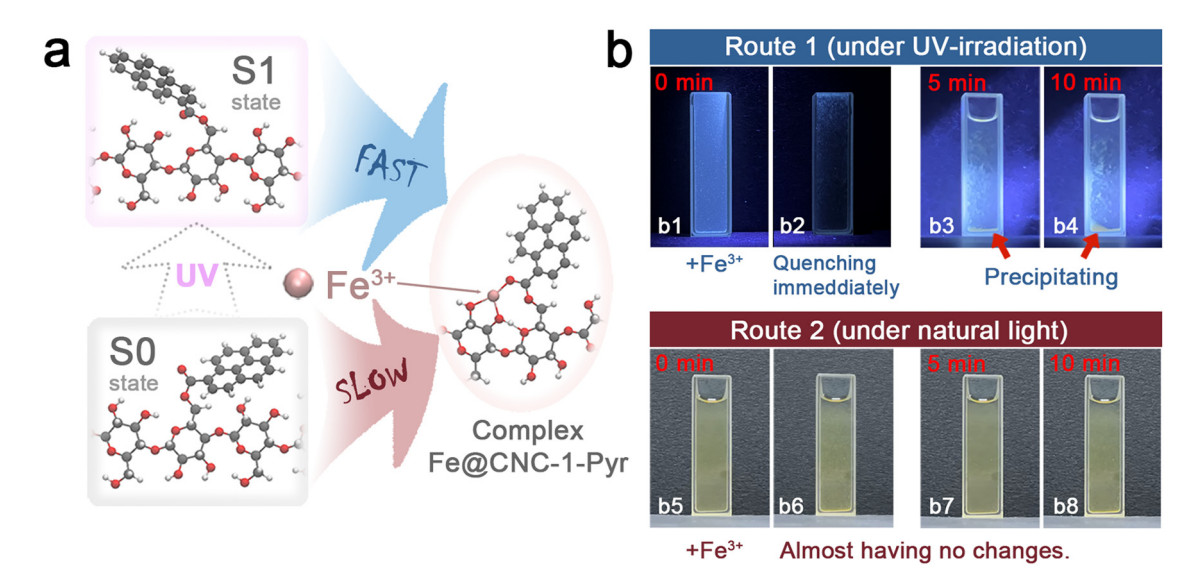


Figure 5: Excited-state geometry relaxation of CNC-1-Pyr for capturing and detecting Fe^{3+} : (a) reaction path for capturing Fe^{3+} and (b) digital photos of CNC-1-Pyr solution mixing with Fe^{3+} solution under (b1-b4) UV light and (b5-b8) natural light.

Fe $^{3+}$ complexation by CNC-1-Pyr does occur under natural light because it is a thermodynamically favorable process, but this process seems to be relatively slow since there is no obvious phenomenon of precipitation even after observation continued for 10 min. The obvious distinction between the two paths is shown in time-lapse videos in the Supporting Information. The differences may originate from significant differences in molecular conformations between SO and S1 states. We notice that the excited S1 state of CNC-1-Pyr and the complex of Fe $^{3+}$ @CNC-1-Pyr are similar. The underlying mechanisms are believed to be that the excited S1 state is more likely to be complex with Fe $^{3+}$ (details in Figure S7), and then forming a

stable structure. As for the SO state, however, a noteworthy structural relaxation is necessary before the possible complexing with Fe³⁺. Therefore, the excitation of UV light seems quite important for generating ion traps for perfectly capturing Fe³⁺ sensitively and specifically.

4 Conclusions

In summary, pyrene-modified CNCs are prepared by onestep esterification, exhibiting potential in detecting and capturing Fe³⁺. In addition, the plenty of hydroxyl groups on the surface of CNC-1-Pyr make them disperse well in water. The results of simulation and experiments show that a remarkable geometry relaxation of CNC-1-Pyr based on the rotation of ester bonds occurs under UV-light excitation. The excited S1 state seems quite suitable for capturing Fe^{3+} , leading to obvious fluorescence quench. This unique feature endows CNC-1-Pyr dual function of selectively detecting and efficiently capturing Fe^{3+} . The LOD of Fe^{3+} is as low as 0.3374 μ mol/L and there is good linear relationship between the maximum fluorescent intensity and the concentration of Fe^{3+} in the range of 1–1,000 μ mol/L. Besides, this unusual phenomenon may have important implications for the further exploration of the possible photo-isomerization effect and mechanism of CNC-1-Pyr or similar structures.

Acknowledgments: The authors express their gratitude to Edit Springs (https://www.editsprings.cn/) for the expert linguistics provided.

Funding information: The authors acknowledge the financial support provided by the National Natural Science Foundation of China (No. 51772251) and the Science and Technology Planning Project of Sichuan Province (Nos. 2021ZYD0053, 2020YFN0150 and 2020ZDZX0008).

Author contributions: All authors have accepted responsibility for the entire content of this manuscript and approved its submission.

Conflict of interest: The authors state no conflict of interest.

Data availability statement: The data that support the findings of this study are available from the corresponding author upon reasonable request.

References

- [1] PhilipAisen P, ALeibold E. Iron metabolism. Curr Opin Chem Biol. 1999;3(2):200-6.
- [2] Guo Q, Li L, Hou S, Yuan Z, Li C, Zhang W, et al. The role of iron in cancer progression. Front Oncol. 2021;11:778492.
- [3] Lee S, Bong S, Ha J, Kwak M, Park S-K, Piao Y. Electrochemical deposition of bismuth on activated graphene-nation composite for anodic stripping voltammetric determination of trace heavy metals. Sens Actuators B Chem. 2015;215:62–9.
- [4] Aydin FA, Soylak M. Separation, preconcentration and inductively coupled plasma-mass spectrometric (ICP-MS) determination of thorium(IV), titanium(IV), iron(III), lead(II) and chromium(III) on 2-nitroso-1-naphthol impregnated MCI GEL CHP20P resin. J Haz Mat. 2010;173(1–3):669–74.

- [5] Špirić Z, Vučković I, Stafilov T, Kušan V, Frontasyeva M. Air pollution study in croatia using moss biomonitoring and ICP-AES and AAS analytical techniques. Arch Environ Con Tox. 2013;65(1):33–46.
- [6] Nawaz H, Tian W, Zhang J, Jia R, Chen Z, Zhang J. Cellulose-based sensor containing phenanthroline for the highly selective and rapid detection of Fe²⁺ ions with naked eye and fluorescent dual modes. ACS Appl Mater Inter. 2018;10(2):2114–21.
- [7] Park S-H, Kwon N, Lee J-H, Yoon J, Shin I. Synthetic ratiometric fluorescent probes for detection of ions. Chem Soc Rev. 2020;49(1):143-79.
- [8] Rajar K, Alveroglu E. CNTs based water soluble fluorescent sensor for selective detection of Fe³⁺ ion. Mater Res Bull. 2020:124:110748.
- [9] Zhou Y, Zheng H, Kravchenko II, Valentine J. Flat optics for image differentiation. Nat Photonics. 2020;14(5):316–23.
- [10] Murugan B, Sagadevan S, Fatimah I, Oh WC, Hossain MA, Johan MR. Smart stimuli-responsive nanocarriers for the cancer therapy-nanomedicine. Nanotechnol Rev. 2021;10(1):933-53.
- [11] Visconti P, Primiceri P, Fazio Rd, Strafella L, Ficarella A, Carlucci AP. Light-induced ignition of carbon nanotubes and energetic nano-materials: a review on methods and advanced technical solutions for nanoparticles-enriched fuels combustions. Rev Adv Mater Sci. 2020;59(1):26–46.
- [12] Song RY, Zhang Q, Chu YL, Zhang L, Dai HQ, Wu WB. Fluorescent cellulose nanocrystals for the detection of lead ions in complete aqueous solution. Cellulose. 2019;26(18):9553-65.
- [13] Weishaupt R, Siqueira G, Schubert M, Kämpf MM, Zimmermann T, Maniura-Weber K, et al. A protein-nanocellulose paper for sensing copper ions at the nano- to micromolar level. Adv Funct Mater. 2017;27(4):1604291.
- [14] Hou P, Wang J, Fu S, Liu L, Chen S. A new turn-on fluorescent probe with ultra-large fluorescence enhancement for detection of hydrogen polysulfides based on dual quenching strategy. Spectrochim Acta A Mol Biomol Spectrosc. 2019;213:342-6.
- [15] Sîrbu E, Eyley S, Thielemans W. Coumarin and carbazole fluorescently modified cellulose nanocrystals using a one-step esterification procedure. Can J Chem Eng. 2016;94(11):2186–94.
- [16] Tian H, Dai Y, Fu W, Liu H, Li M, Lv M, et al. Dansyl-modified carbon dots with dual-emission for pH sensing, Fe³⁺ ion detection and fluorescent ink. RSC Adv. 2020;10(61):36971-9.
- [17] Tian W, Zhang J, Yu J, Wu J, Nawaz H, Zhang J, et al. Cellulose-based solid fluorescent materials. Adv Opt Mater. 2016;4(12):2044-50.
- [18] Ayyavoo K, Velusamy P. Pyrene based materials as fluorescent probes in chemical and biological fields. N J Chem. 2021;45(25):10997-1017.
- [19] Usman K, Islam A, Ullah Shah SH, Javaid K, Amin A, Mustafa Z, et al. Fluorescent pyrene-imidazole material for deep-blue organic light-emitting devices. Opt Mater. 2021;121:111582.
- [20] Bai CB, Xu P, Zhang J, Qiao R, Chen MY, Mei MY, et al. Long-wavelength fluorescent chemosensors for Hg²⁺ based on pyrene. ACS Omega. 2019;4(11):14621-5.
- [21] Zhou Y, Kravchenko II, Wang H, Zheng H, Gu G, Valentine J. Multifunctional metaoptics based on bilayer metasurfaces. Light: Sci Appl. 2019;8(1):80.

- [22] Zhou Y, He X-T, Zhao F-L, Dong J-W. Proposal for achieving in-plane magnetic mirrors by silicon photonic crystals.

 Opt Lett. 2016;41(10):2209-12.
- [23] Ye X, Wang HY, Yu LS, Zhou JP. Aggregation-induced emission (AIE)-labeled cellulose nanocrystals for the detection of nitrophenolic explosives in aqueous solutions. Nanomaterials. 2019;9(5):707.
- [24] Zhang L, Li Q, Zhou J, Zhang L. Synthesis and photophysical behavior of pyrene-bearing cellulose nanocrystals for Fe³⁺ sensing. Macromol Chem Phys. 2012;213(15):1612-7.
- [25] Frisch MJ, Trucks GW, Schlegel HB, Scuseria GE, Robb MA, Cheeseman JR, et al. Gaussian 16 Rev. C.01. Wallingford, CT: 2016.
- [26] Lu T, Chen FW. Multiwfn: a multifunctional wavefunction analyzer. J Comput Chem. 2012;33(5):580-92.
- [27] Humphrey W, Dalke A, Schulten K. VMD: visual molecular dynamics. J Mol Graph Model. 1996;14(1):33–8.
- [28] Yu T, Soomro SA, Huang F, Wei W, Wang B, Zhou Z, et al. Naturally or artificially constructed nanocellulose architectures for epoxy composites: a reviews. Rev Adv Mater Sci. 2020;9(1):1643–59.
- [29] Chanda S, Bajwa DS. A review of current physical techniques for dispersion of cellulose nanomaterials in polymer matrices. Rev Adv Mater Sci. 2021;60(1):325-41.

- [30] Tian W, Zhang J, Yu J, Wu J, Zhang J, He J, et al. Phototunable full-color emission of cellulose-based dynamic fluorescent materials. Adv Funct Mater. 2018;28(9):1703548.
- [31] Li W, Tan L, Fan QD, Wei W, Zhou ZW. Effect of storage time and temperature on dissolved state of cellulose in TBAH-based solvents and mechanical property of regenerated films. Rev Adv Mater Sci. 2021;60(1):466-78.
- [32] Zeng YL, Jiang L, Cai XY, Li Y. Identification of the characteristic vibrations for 16 PAHs based on Raman spectrum. Spectrosc Spect Anal. 2014;34(11):2999–3004.
- [33] Thompson L, Azadmanjiri J, Nikzad M, Sbarski I, Wang J, Yu A. Cellulose nanocrystals: production, functionalization and advanced applications. Rev Adv Mater Sci. 2019:58(1):1–16.
- [34] Zhang YJ, Ma XZ, Gan L, Xia T, Shen J, Huang J. Fabrication of fluorescent cellulose nanocrystal via controllable chemical modification towards selective and quantitative detection of Cu(II) ion. Cellulose. 2018;25(10):5831–42.
- [35] Zhang H, Chen G, Yu B, Cong H. Emerging advanced nanomaterials for cancer photothermal therapy. Rev Adv Mater Sci. 2018;53(2):131–46.
- [36] Yang X, Zhang D, Ye Y, Zhao Y. Recent advances in multifunctional fluorescent probes for viscosity and analytes.

 Coord Chem Rev. 2022;453:214336.